J Mol Model (2014) 20:2491
DOI 10.1007/s00894-014-2491-2

ORIGINAL PAPER

Understanding the effects on constitutive activation and drug binding of a D130N mutation in the β2 adrenergic receptor via molecular dynamics simulation

Yanyan Zhu · Yuan Yuan · Xiuchan Xiao · Liyun Zhang · Yanzhi Guo · Xuemei Pu

Received: 16 May 2014 / Accepted: 6 October 2014 / Published online: 25 October 2014

Abstract G-protein-coupled receptors (GPCRs) are currently one of the largest families of drug targets. The constitutive activation induced by mutation of key GPCR residues is associated closely with various diseases. However, the structural basis underlying such activation and its role in drug binding has remained unclear. Herein, we used all-atom molecular dynamics simulations and free energy calculations to study the effects of a D130N mutation on the structure of β2 adrenergic receptor (β2AR) and its binding of the agonist salbutamol. The results indicate that the mutation caused significant changes in some key helices. In particular, the mutation leads to the departure of transmembrane 3 (TM3) from transmembrane 6 (TM6) and marked changes in the NPxxY region as well as the complete disruption of a key ionic lock, all of which contribute to the observed constitutive activation. In addition, the D130N mutation weakens some important H-bonds, leading to structural changes in these regions. Binding free energy calculations indicate that van der Waals and electrostatic interactions are the main driving forces in binding salbutamol; however, binding strength in the mutant β2AR is significantly enhanced mainly through modifying electrostatic interactions. Further analysis revealed that the increase in binding energy upon mutation stems mainly from the H-bonds formed between the hydroxyl group of salbutamol and the serine residues of TM5. This observation suggests that modifications of the H-bond groups of this drug could significantly influence drug efficacy in the treatment of diseases associated with this mutation.

Keywords G-protein-coupled receptor · Mutation · Molecular dynamics simulation · Agonist

Introduction

The superfamily of G-protein coupled receptors (GPCRs) is the largest known family of membrane proteins and is characterized by the presence of seven transmembrane (TM) helical segments [1, 2]. Based on sequence similarity, GPCRs can be classified into six subfamilies: A, B, C, D, E, F. GPCRs have become the largest family of drug targets, being targeted by around 30% of currently marketed drugs [3]. Activation of GPCRs is considered the most important mode of regulating signal transduction via interaction with both membrane- and G-proteins.

The binding of particular drugs to native GPCRs can lead to receptor activation [4]; however, it was found that GPCRs are also activated by some mutations even without agonist binding. In other words, they can become constitutively active. Such mutation-induced constitutive activation is associated closely with various disease states (e.g., oncogenesis) [5, 6]. A point mutation of a highly conserved proline to histidine in rhodopsin, causing the disease retinitis pigmentosa, was first reported in 1990 [7]. Mutations at Gly90 and Lys296 of rhodopsin were observed to be associated with congenital night blindness [8] and retinitis pigmentosa [9], respectively. The constitutive activation of luteinizing hormone receptor induced by mutations located mainly in the TM6 region and in the C-terminal part of the 3rd extracellular loop (ECL) was considered responsible for familial male precocious puberty [10]. Other examples include familial non-autoimmune

Electronic supplementary material The online version of this article (doi:10.1007/s00894-014-2491-2) contains supplementary material, which is available to authorized users.

Y. Zhu · X. Xiao · L. Zhang · Y. Guo · X. Pu (✉)
Faculty of Chemistry, Sichuan University, No. 29 Jiuyanqiao Wangjiang Road, Chengdu 610064, People's Republic of China
e-mail: xmpuscu@scu.edu.cn

Y. Yuan
College of Management, Southwest University for Nationalities, Chengdu 610041, People's Republic of China

hyperthyroidism and hyperfunctional thyroid nodules, which were reported to be associated with somatic and germline mutations of the thyrotropin receptor (such as I486F, T632I and C672Y etc.) [11].

Given the above, in the field of drug design it is very important to understand the activation mechanism induced by both drugs and receptor mutations. Although significant progress has been made in understanding the structural basis of drug-induced activation during the past few years, mainly from comparison of active and inactive receptor structures that have been solved experimentally, detailed mechanisms of activation are yet to be explained clearly, in particular activation associated with mutation. The experimental difficulty of determining GPCR structure means that it is still challenging to explore the activation mechanism for this large receptor family. To date, only very few GPCR structures have been solved successfully [12–15], which significantly limits structure-based GPCR drug discovery strategies. Taking an alternative approach, computational modeling has become an effective way to provide valuable insights into the structure and function of GPCRs in the absence of experimental structural data.

Among reported GPCR mutations, mutations of key residues located in the highly conserved DRY motif of β2 adrenergic receptor (β2AR)—the first human GPCR structure to be solved—were revealed to play an extremely important role in breaking its inactive state [16, 17]. The DRY motif of β2AR is composed of Asp130$^{3.49}$, Arg131$^{3.50}$ and Tyr141^{ICL2}. Mutation of conserved Asp130$^{3.49}$ to Asn (viz., D130N mutation) (see Fig. 1) in the DRY motif was found to result in the constitutive activation of β2AR, significantly influencing its binding with agonist drugs [16]. However, because no crystal structure is available for the mutated structure, our understanding of the basis of the D130N mutation-induced activation mechanism and changes in drug binding remains very limited [16].

Molecular dynamics (MD) simulations have been used successfully to study the structure and function of proteins to obtain microscopic information at the molecular level and to supplement experimental investigations [18–22], including study of GPCRs [23, 24]. Previous MD studies on GPCRs have focused largely on the effects of ligand binding. But MD simulations of GPCR mutants have been lacking so far, despite the fact that such information is also of particular importance for understanding the structure and function of wild type GPCRs.

Therefore, in the present work, we employed MD simulation to study how the D130N mutation in inactive β2AR induces its activation. In addition, we performed binding free energy calculations to gain insights into the effect of the mutation on drug binding. A β2AR-specific agonist (salbutamol) was selected as a representative drug due to the experimental findings that the D130N mutation could enhance binding of this agonist. The observations from this work will provide valuable information for understanding mutation-induced constitutive activation mechanisms and related drug design.

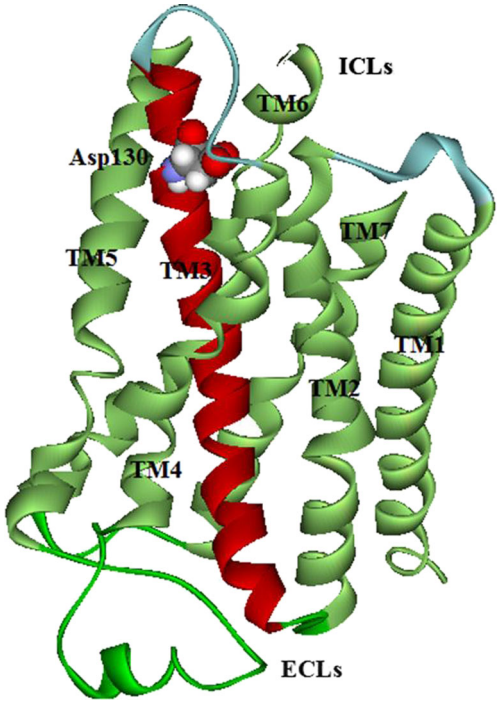

Fig. 1 Illustration of β2 adrenergic receptor (β2AR) structure. *Ball model* Mutated Asp130$^{3.49}$ residue

Materials and methods

Structure preparation

The X-ray crystal structure of human β2AR (Protein Data Bank ID code 2RH1) bound to carazolol was used in this work to construct the initial coordinates for the inactive β2AR structure [viz., the wild type (WT)]. Because carazolol is an inverse agonist, 2RH1 could represent a nearly inactive state of the β2AR receptor. The crystal structure contains one β2AR receptor and certain small molecules. It was reported that these small molecules have no obvious effect on β2AR structure and function [25]. Thus, we removed them to simplify the simulation. In addition, the T4 lysozyme protein in the crystal structure was also removed since its rigidity may affect the structure and dynamic behavior of β2AR [25]. Thus, only 276 residues were used to model WT β2AR. The D130N mutation structure was constructed using Swiss-Pdbviewer [26] software, based on the WT model above. The prepared protein was then inserted into a well prepared phospholipid bilayer: palmitoyl oleoyl phosphatidyl choline (POPC) [27]. Chloride ions were introduced to neutralize the protein charge using columbic potential terms. Water

molecules were added using the Xleap utility. The rectangle periodic box was set up so that any solute atom was at least 10 Å from any box edges. As a result, the systems contain 34,711 water molecules for the WT and 32,115 for the mutant receptor.

Molecular dynamics simulation

The AMBER03 [28] force field was used for the receptor, and water was represented by the TIP3P [29] model. The GAFF [30] force field was utilized for POPC. MD simulations were performed using the Sander module of the AMBER12.0 package.

To remove bad contacts in the initial geometries of the two systems, four energy minimizations were performed using the same procedure: 20,000 steps for the solvent molecules followed by 20,000 steps for the POPC, and 20,000 steps for the receptor, finally, 20,000 steps for the whole system. After the minimizations, the systems were heated from 0 to 300 K within 120ps. Then, 5 ns MD simulations were carried out with periodic boundary conditions in the NVT ensemble at 300 K using Berendsen temperature coupling [31]. Finally, 105 ns NPT simulations (T = 300 K and P = 1 atm) were performed in the canonical ensemble. The SHAKE algorithm [32] was applied to constrain all bonds involving a hydrogen atom with a tolerance of 1.0×10^{-5} Å. Nonbond interactions were handled with a 10 Å atom-based cutoff. The particle-mesh-Ewald (PME) method [33, 34] was applied to treat long-range electrostatic interactions. For analysis, the trajectories were saved at an interval of 2 ps in the MD simulations. All the MD results were analyzed using the analysis module of AMBER 12.0 and VMD [35] as well as some other specifically developed trajectory analysis software.

Binding free energy calculation

Using Autodock 4.2 [36] software, the agonist salbutamol was docked into the MD equilibrium structures of WT and mutated β2AR, respectively; 20 ns MD simulations were further carried out for the docked complex. The GAFF force field was utilized for the agonist, which was allocated using the AMTECHAMBER module [37]. For the energy analysis, some snapshots without water molecules and chloride ions were extracted from the MD trajectory. The molecular mechanics generalized Born surface area (MM/GBSA) [38] approach integrated in AMBER 12 was applied to these snapshots to obtain the binding free energy, using Eq. (1).

$$\Delta G_{\text{binding}} = G_{\text{complex}} - \left(G_{\text{receptor}} + G_{\text{ligand}}\right) \quad (1)$$

Where G_{complex}, G_{receptor} and G_{ligand} denote the free energies of the complex, β2AR, and the ligand, respectively. The free energies were estimated as the sum of the four terms in Eq. (2).

$$G = E_{\text{gas}} - TS + G_{\text{psolv}} + G_{\text{npsolv}} \quad (2)$$

Where E_{gas} is the molecular mechanical gas phase energy, calculated as the sum of electrostatic energy (ΔE_{ele}) and the van der Waals interactions (ΔE_{vdw}). G_{psolv} represents the polar contribution to the solvation energy, while G_{npsolv} is the nonpolar contribution to the solvation energy of the molecular. T is the absolute temperature and S is the molecular entropy. Similar to many other studies, the change in solute entropy was not considered in the calculation of the free energies since we were focused on the relative order of binding free energy [39, 40].

The polar contribution to the solvation energy of the molecular was calculated by the GB model (IGB = 2) and the nonpolar contribution was determined on the basis of solvent-accessible surface area (SASA) using the LCPO method [see Eq. (3)].

$$\Delta G_{\text{npsolv}} = 0.072 \ \ \Delta SASA \quad (3)$$

The constants of interior dielectric and the solvent were set to 1 and 80, respectively.

Results and discussion

Overall structures of WT and mutated β2AR

Root mean square deviations (RMSDs) from the inactive crystal structure were calculated for the backbone atoms (Cα) of WT and mutated β2AR (Fig. 2), and served as one indicator to describe the mutation effect on the overall structure. As can be seen from Fig. 2, the RMSD value of the mutant is larger than that of the WT over the last 30 ns of the simulation time, as confirmed by Student's t-test ($P<0.05$). Student's t-test is a statistical method commonly used for examining if there is significant difference between two sets of data in terms of a comparison of the calculated P-value with the cutoff value (0.05). The observation indicates that the mutation of the conserved $\text{Asp130}^{3.49}$ to Asn would decrease the stability of the inactive β2AR, consistent with experimental findings reported by Rasmussen in 1999 [16].

In addition, the radius of gyration (R_g) for the Cα atoms of each β2AR were calculated and are shown in Fig. 2. It is clear that the R_g values in the WT and mutant systems are very similar. This observation suggests that the mutation of the highly conserved aspartic acid residue in the inactive β2AR

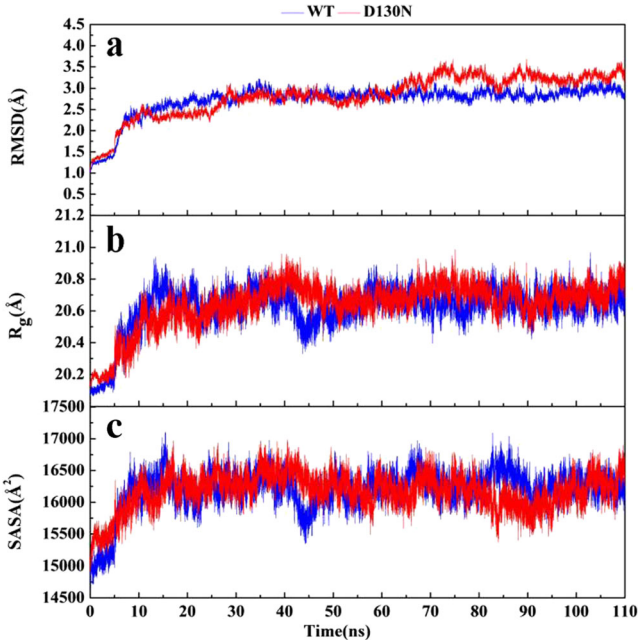

Fig. 2 Changes in **a** root mean square deviations (RMSD; in Å) values of backbone atoms and **b** the radius of gyration (R_g, in Å) as well as **c** the solvent-accessible surface area (SASA, in Å^2) as functions of simulation times for wild type (WT) and mutant (D130N) β2AR. The RMSD value represents deviation from the inactive crystal structure

to the neutral asparagine acid residue plays a negligible role in governing the compactness of the overall structure of the receptor. The caculated SASA (see Fig. 2) shows no apparent difference between the WT and the D130N mutant, similar to the radius of gyration and further confirming the negligible effects of the mutation on the compactness of the receptor.

Structural changes in local regions

To gain insight into the effects of the mutation on local structures within β2AR, we also calculated the RMSD value of each residue in terms of the last 10 ns trajectories. As shown in Fig. 3, the RMSD values of most residues were larger in the mutant system than those in the WT, in accordance with the change trend of the total RMSD values above.

The GPCR structure is known to be composed of seven TM helical segments connected by intracellular (ICL) and extracellular (ECL) loops. Inspection of Fig. 3 shows that the RMSD values of most residues located in the five helixes (viz., TM2, TM3, TM5, TM6 and TM7) are larger in the mutant system than those in the WT, suggesting that the mutation induces significant deviations from the inactive crystal structure and destabilizes the structure of the five helixes. In contrast, the mutation leads to smaller RMSD values for most residues located in the TM1 and TM4 regions, to some extent stabilizing the structure of the two regions.

As revealed by Fig. 3, residues with high RMSD values, and the large differences in the RMSD values between the

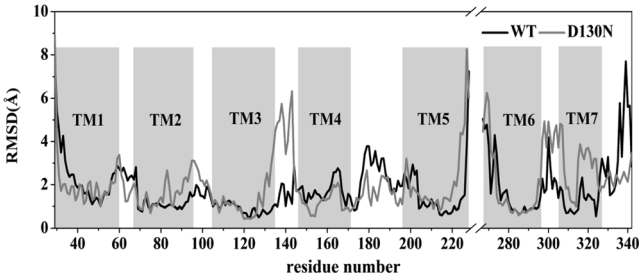

Fig. 3 A comparison of average RMSD values (in Å) per residue between WT and mutant β2AR (D130N) over the last 10 ns trajectories. Residues corresponding to the seven transmembrane helices (TM1–TM7) are highlighted in *gray*. The RMSD value is for deviation from the active crystal structure

mutant and WT systems are located mainly in the TM2, TM3, TM5 and TM7 regions. For example, the residues at the ends of TM2, TM3 and TM5 exhibit much higher RMSD values and larger RMSD deviations than the other parts of the receptor in the mutant system. The mutated Asp130$^{3.49}$ residue is located at the terminus of TM3. Thus, this region exhibits significant structural changes. Interestingly, the RMSD values of all TM7 residues in the mutant β2AR exhibited much larger deviations from the WT system than those of the other helices. The G-protein-binding-site is located in the ICL of β2AR, adjacent to the NPxxY region (Asn322$^{7.49}$–Tyr326$^{7.53}$) [41]. An inspection of Fig. 3 and the *P* value calculated by Student's *t*-test ($P<0.05$) indicate that the RMSD values of the NPxxY region are significantly higher in the mutant than in the WT. The NPxxY motif is highly conserved in the subfamily of GPCR, and is thought to be closely related with the process of G protein binding and important for maintaining the structures of the inactive state [3]. Thereby, the high RMSD values in this region suggest that the mutation may trigger instability of the highly conserved NPxxY region in TM7, which would contribute to the constitutive activation observed with the single point mutation. In addition, Fig. 3 clearly shows that the highest RMSD deviations between the two systems are located in residues Ser137^{ICL2}–Thr146^{ICL2}, which are not included in the seven helices but belong to the ICL2 region. ICL2 is located in the region adjacent to the mutated Asp130 residue, thus leading to significant changes in structure. As revealed by Fig. 3, the conformations of TM2, TM6 and TM7 also incur significant changes, although they are located far from the Asp130$^{3.49}$ mutation site. This observation indicates that the particular mutation not only induces conformational changes not only of adjacent regions, but also regions relatively far from the mutated residue.

Ionic lock

The ionic lock formed between the charged residues Arg131$^{3.50}$ (located in the DRY motif) and Glu268$^{6.30}$, has

Table 1 Comparison of ionic lock conformations in some G-protein-coupled receptor (GPCR) crystal structures

PDB ID	Protein	C_α–C_α(Å)[a]	Note[b]
2RH1	β2AR	11.2	T4L fusion
3D4S	β2AR	11.0	T4L fusion
1U19	Rhodopsin	9.1	Inactive
1GZM	Rhodopsin	8.7	Inactive

[a] The C_α–C_α distances (between the C_α atom of $Arg^{3.50}$ and $Glu^{6.30}$) in the inactive crystal β2 adrenergic receptor (β2AR) structures are greater than those in inactive rhodopsin receptors

[b] The β2ARs were determined with bound inverse agonists or antagonists (carazolol for 2RH1 and timolol for 3D4S)

been considered to be important to maintain rhodopsin [9], alpha(1b) adrenergic receptor [42], and the delta opioid receptors of δ and μ [43, 44] in their inactive states. Switching of GPCRs from an inactive to an active state may involve breaking of this critical ionic lock.

Indeed, the ionic lock is found in the crystal structure of inactive rhodopsin [45]. A value of 9.0–9.5 Å, which is close to the distance of the ionic lock in the inactive rhodopsin structure (see Table 1), is often taken as a reference to evaluate the existence of the ionic lock in other GPCRs [46]. However, using this reference value, the reported ionic lock cannot be found in the crystal structure of the inactive β2AR (Table 1). However, it is unreasonable to conclude that the inactive β2AR has no the ionic lock only in terms of information from the crystal structure. Clearly, the crystal structure represents only a static snapshot while the protein is a dynamic structure.

We next inspected the dynamic behavior of the reported ionic lock in WT β2AR and its changes upon the mutation (see Fig. 4). As can be seen from Fig. 4, the ionic lock in WT β2AR exists intermittently within the simulation time. Sometimes it is formed and sometimes it is broken, displaying to some extent an equilibrium between conformations with ionic lock formed or broken. This observation indicates that it is not essential for WT β2AR to possess a stable ionic lock in its inactive state, consistent with findings from some non-rhodopsin GPCRs [47]. The *P* value calculated by Student's *t*-test ($P<0.05$) further confirms that the distance between $Arg131^{3.50}$ and $Glu268^{6.30}$ is significantly increased in the mutated β2AR relative to the WT system. The distance reaches a value of almost 12 Å over the whole simulation time, as shown in Fig. 4b. This result suggests that the ionic lock is broken completely due to the mutation.

In addition, we also examined the change in distance between the two helices associated with the ionic lock (viz., TM3 and TM6) since their conformational changes have been suggested to be critical for GPCR activation [48, 49]. As can be seen from Fig. 5, the D130N mutation leads to a significant increase in the distance between the two helices and the *P* value calculated by Student's *t*-test ($P<0.05$) further confirms that the increase is significant. Figure 4b also clearly displays the moving apart of the ends of TM3 and TM6 in the mutated receptor. This observation provides further support for the experimental finding that disruption of the special ionic lock can be characterized by the separation of TM3 and TM6 [50]. Since experimental investigations have revealed that activation of GPCRs involves breaking of the critical ionic lock, the D130N mutation should favor β2AR approaching the active state and would lead to constitutive activity.

H-bonding

Since H-bonds play an important role in maintaining the structure and function of proteins, we analyzed H-bonding in the WT and mutant systems. Table 2 lists some representative H-bonds between the seven helices with a lifetime above 30% of the simulation time (see supporting information Table S1 for more H-bonds). In the WT system, the total number of H-bonds was calculated to be 20, with 18 in the

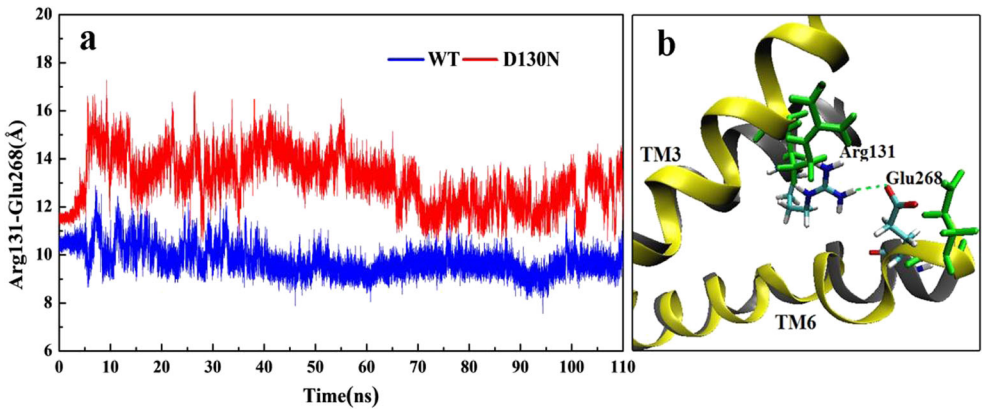

Fig. 4 **a** Time-dependent changes in the salt bridge distances (Å) formed between $Arg131^{3.50}$ and $Glu268^{6.30}$ residues for WT and mutant β2AR (D130N). **b** Superimposition of two representative conformations from WT (*gray*) and mutant (*yellow*) β2AR. The ionic lock residues ($Arg131^{3.50}$ and $Glu268^{6.30}$) for WT are colored according to atom type: *cyan* C, *red* O, *white* H, *blue* N, *green* two residues in D130N. *Green dotted line* H-bonding

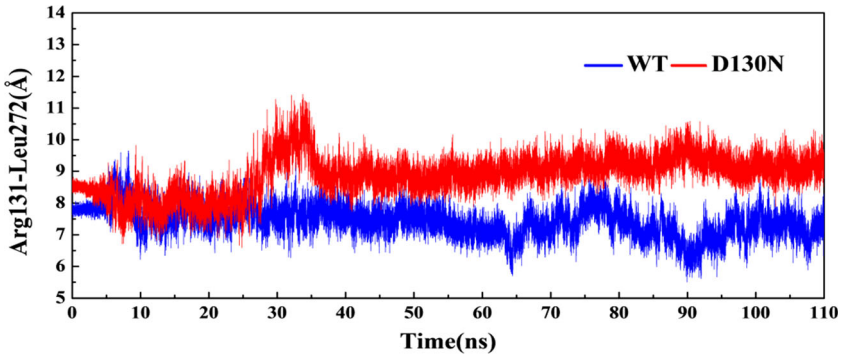

Fig. 5 Time-dependent changes in the distance between helices TM3 and TM6 for WT and mutant β2AR (D130N), as represented by the distance between C_α atoms of Arg131$^{3.50}$ and Leu272$^{6.34}$ residues

mutant system. Although the number of H-bonds displays minor difference between the two systems, the residues involved in H-bonding are significantly different, as can be seen from Table 2. This difference further confirms the structural changes induced by the mutation.

Inspection of Table 2 reveals two very stable H-bonds between Asp130$^{3.49}$ and Arg131$^{3.50}$ residues in the WT system, with 100% lifetime. The mutation weakens the H-bonding to some extent because the lifetime drops to 87–92% in the mutant form. Furthermore, the two H-bonds are formed between OD2@ Asp130$^{3.49}$ atom and the Arg131$^{3.50}$ residue in the WT, while it is the OD1@ Asp130$^{3.49}$ atom rather than OD2@Asp130$^{3.49}$ that forms the two H-bonds with the Arg131$^{3.50}$ residue in the mutant system, as shown in Table 2. These observations provide further support for the structural changes in the DRY region induced by the mutation. Interestingly, there are nearly no stable H-bonds between TM3 and TM6 in the WT, in which the highest lifetime is observed to be about 24% for the H-bond between Glu268$^{6.30}$ and Arg131$^{3.50}$ residues (viz., the ionic lock residues). Furthermore, the unstable H-bond disappears completely in the mutant system, consistent with disruption of the ionic lock formed between the two residues, as observed above.

Table 2 Average distances of some representative hydrogen bonds (Å) formed between the seven helices and their percentage occupation (%) for the WT and mutated β2AR (D130N) over the last 10 ns trajectories

System	WT (%/Å)	D130N (%/Å)
OD2@Asp79$^{2.50}$···OG@ Ser 319$^{7.46}$	100/2.69	73/2.74
OD1@ Asp79$^{2.50}$ ···ND2@ Asn 322$^{7.49}$	99/2.94	0%
OD1@ Asp79$^{2.50}$ ···OH@ Tyr 326$^{7.53}$	99/2.78	0%
OD2@ Asp79$^{2.50}$···ND2@Asn 322$^{7.49}$	81/3.16	0%
OD1@ A Asp79$^{2.50}$···OG@ Ser 319$^{7.46}$	0%	70/2.97
OD2@ Asn130$^{3.49}$···NH2@ Arg131$^{3.50}$	100/2.78	0%
OD2@ Asn130$^{3.49}$···NE@ Arg131$^{3.50}$	99/2.93	0%
OD1@ Asn130$^{3.49}$···NH2@ Arg131$^{3.50}$	0%	92/2.90
OD1@ Asn130$^{3.49}$···NE@ Arg131$^{3.50}$	0%	87/3.09
OE2@ Glu268$^{6.30}$···NH1@ Arg131$^{3.50}$	24%	0%

As shown, H-bonding between TM2 and TM7 is crucial in stabilizing the inactive structure of β2AR [51]. Some H-bond interactions involving highly conserved residues, including Asn51$^{1.50}$, Asp79$^{2.50}$, Ser319$^{7.46}$ Asn322$^{7.49}$ and Tyr326$^{7.53}$, were reported in mutagenesis [52–55] and some limited MD studies [56] to be important for receptor activation. The data in Table 2 show that the mutation reduces the number of H-bonds between TM7 and TM2. The stable hydrogen bonds at Asp79$^{2.50}$–Ser319$^{7.46}$, Asp79$^{2.5}$–Asn322$^{7.49}$ and Asp79$^{2.50}$–Tyr326$^{7.53}$ are almost destroyed upon the conformational change induced by the D130N mutation. Although an additional H-bond between OD1@Asp79$^{2.50}$ and OG@Ser319$^{7.46}$ is formed over 70% simulation time in the mutant system, the mutation-weakened H-bonding between TM2 and TM7 would lead to significant structural changes in the two regions. As evidenced by Fig. 6, TM7 migrates distinctly in the presence of the mutation. As a result, most residues in TM7 exhibit high RMSD values, in particular the NPxxY region involved in H-bonding.

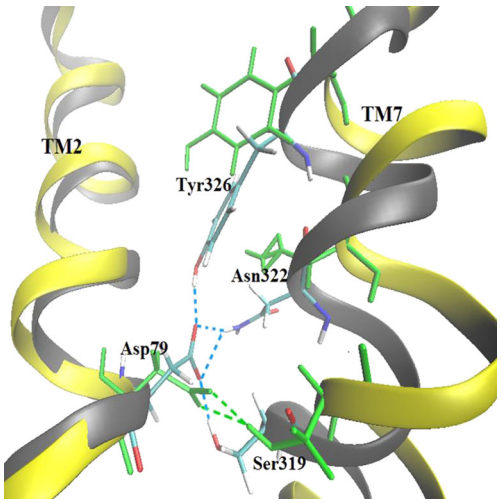

Fig. 6 Structural superimposition of representative conformations of WT (*gray*) and mutant (*yellow*) β2AR. Crucial residues Asp79$^{2.50}$, Ser319$^{7.46}$ Asn322$^{7.49}$ and Tyr326$^{7.53}$ for WT β2AR are colored according to atom type: *cyan* C, *red* O, *white* H, *blue* N, *green* four residues in the mutated β2AR. The *blue* and *green dotted lines* denote H-bonding for the WT and mutant systems, respectively

On the whole, the differences in H-bond interactions between the WT and mutant systems provide further support for transformation of helix structures upon the mutation, for example, the departure of TM3 from TM6 as well as TM7 from TM2. These changes upon mutation are consistent with some experimental observations from the D130N mutation [16].

MM/GBSA binding free energy calculation

To gain insight into the effect of the D130N mutation on the interaction between the β2AR receptor and cognate drugs, we selected salbutamol (a specific agonist of β2AR) to study its interaction with WT and mutated β2ARs. Salbutamol (Fig. 7) is an effective drug used to treat conditions such as primary bronchial asthma [57] and cardiovascular disease [58], etc. Salbutamol was docked into the MD equilibrium structures of WT and mutated β2AR, respectively. Then, 20 ns classical MD simulations were carried out for the two complex systems. For the energy analysis, 100 snapshots without water and chloride ions were extracted from the last 10 ns trajectory at 100 ps interval. Binding free energies were calculated using the molecular mechanics generalized Born/surface area (MM/GBSA) method.

Table 3 lists the binding free energy and its components. Negative energy term values denote spontaneous interactions favoring binding while positive values have the opposite meaning. Thus, negative $\Delta G_{\text{binding}}$ values indicate that binding between the agonist and the receptor occurs in both the WT and mutant systems. Table 3 clearly shows that the mutation alters the total binding free energies from −35.42 to −45.23 kcal mol^{-1}, significantly enhancing the interaction of β2AR with salbutamol and providing further support for the experimental finding that the D130N mutation increases agonist affinity [16, 59].

To reveal the driving force for the binding free energy, the contribution of each energy component was also analyzed here. The data in Table 3 indicate that non-bonded electrostatic interactions (ΔE_{ele}) and van der Waals interactions (ΔE_{vdw}) are the main driving forces underlying binding strength in the two systems. However, the electrostatic interactions are largely offset by the unfavorable electrostatic solvation free energy (ΔG_{psolv}), as observed from Table 3. This is not unexpected, since the electrostatic interaction is generally anti-correlated with the electrostatic solvation free energy [60]. The non-

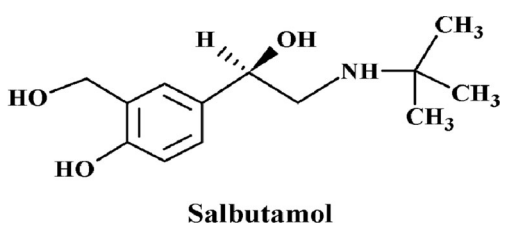

Salbutamol

Fig. 7 Chemical structure of the agonist salbutamol

Table 3 Energetic analysis (kcal mol^{-1}) of the complexes of salbutamol with WT and mutant β2AR (D130N), based on the last 10 ns trajectories

System	WT	D130N
ΔE_{ele}[a]	−21.89±2.68	−43.10±2.58
ΔE_{vdw}[b]	−49.63±4.83	−50.10±4.01
ΔE_{gas}[c]	−71.52±5.54	−93.20±5.36
ΔG_{npsolv}[d]	−4.93±0.10	−4.80±0.14
ΔG_{psolv}[e]	41.03±2.43	52.76±2.15
ΔG_{solv}[f]	36.10±1.92	47.96±1.16
ΔG_{ele}[g]	19.14±1.36	9.66±1.02
$\Delta G_{\text{binding}}$[h]	−35.42±3.40	−45.23±4.07

[a] Non-bonded electrostatic energy contribution estimated by the MM force field

[b] Non-bonded Van der Waals energy calculated through the MM force field

[c] Total free energy in the gas phase

[d] Nonpolar contribution to the solvent free energy

[e] Polar contribution to the solvent free energy

[f] Solvent free energy

[g] Absolute electrostatic energy contribution to the binding free energy

[h] Total binding free energy

$$\Delta E_{\text{gas}} = \Delta E_{\text{ele}} + \Delta E_{\text{vdw}} \quad \Delta G_{\text{solv}} = \Delta G_{\text{psolv}} + \Delta G_{\text{npsolv}}$$
$$\Delta G_{\text{ele}} = \Delta E_{\text{ele}} + \Delta G_{\text{psolv}} \Delta G_{\text{binding}} = \Delta E_{\text{gas}} + \Delta G_{\text{solv}}$$

bonded electrostatic interaction ΔE_{ele} in the wild type was calculated to be −21.89 kcal mol^{-1}, becoming −43.10 kcal mol^{-1} in the mutated form, indicating that the mutation significantly enhances the interaction. However, the van der Waals interactions are almost equal in the two systems (about ~ −50 kcal mol^{-1}). This observation reveals that the mutation significantly increases the binding strength mainly through electrostatic interactions.

Important residues contributing to the binding of salbutamol

In order to further identify the important residues contributing to the binding of salbutamol, the binding energy per-residue was also estimated in terms of Eq. (4).

$$\Delta G_{\text{i-binding}} = G_{\text{i-complex}} - G_{\text{i-receptor}} \tag{4}$$

Where $\Delta G_{\text{i-binding}}$ represents the binding energy of the ith residue, while $G_{\text{i-receptor}}$ and $G_{\text{i-complex}}$ denote the energy of the ith residue in the free and the complexed β2ARs, respectively. The energy of residue i can be estimated from Eq. (5):

$$G_{\text{i-A}} = G_{\text{i-gas}} + G_{\text{i-solv}} \tag{5}$$

In Eq. (5), $G_{\text{i-A}}$ denotes the $G_{\text{i-receptor}}$ or $G_{\text{i-complex}}$ mentioned above. $G_{\text{i-gas}}$ represents the gas phase internal energy of residue i calculated by the AMBER force field. $G_{\text{i-solv}}$ is the solvation energy of the ith residue, including contributions

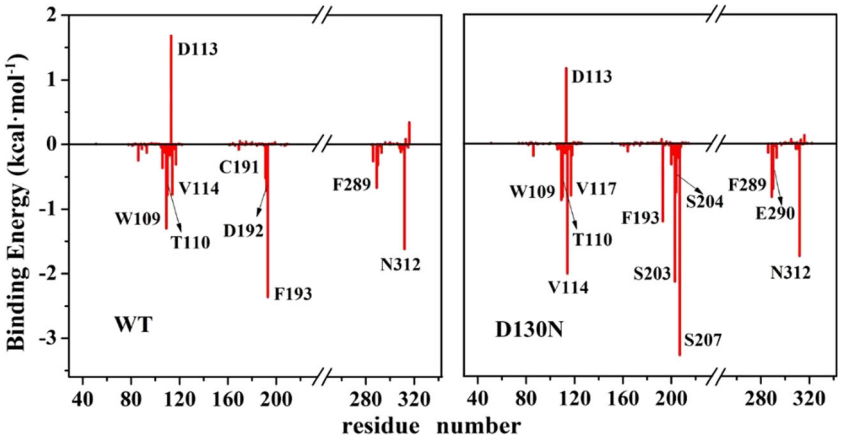

Fig. 8 Per-residue binding energy of $\Delta G_{\text{i-binding}}$ (kcal mol^{-1}) for salbutamol agonist binding WT and mutant β2AR (D130N). Only high energy residues ($|\Delta G_{\text{i-binding}}| \geq 0.5$ kcal mol^{-1}) are shown

from the polar ($G_{\text{i-polar}}$) and nonpolar ($G_{\text{i-nonpolar}}$) terms. The polar contribution is estimated by the GB model and the nonpolar contribution is calculated by Eq. (3) above. Similar to the binding free energy calculation, snapshots without the water molecules and chloride ions were extracted from the last 10 ns MD trajectories at 100 ps intervals for the calculation of binding energy decomposition on a per-residue basis. On the basis of calculated $\Delta G_{\text{i-binding}}$, we could identify residues with significant impact on β2AR-agonist binding (see Fig. 8 and supporting information Tables S2–S3).

In the WT system, eight residues were observed to contribute significantly to the binding of salbutamol with more than 0.5 kcal mol^{-1} free energy contribution (Fig. 8, Table S2). These include three residues in TM3 (Trp109$^{3.28}$, Thr110$^{3.29}$ and Val114$^{3.33}$), three residues in ECL2 (Cys191^{ECL2}, Asp192^{ECL2} and Phe193^{ECL2}), one residue (Phe289$^{6.51}$) in TM6 and residue Asn312$^{7.39}$ in TM7. These residues correspond to the amino acids involved in the binding site revealed by crystal structures of β2AR with diverse ligands bound [61]. Data in Fig. 9 and Table S2 further reveal that these residues contribute to the affinity mainly through van der Waals interactions. For example, the aromatic residue Phe193^{ECL2} is able to interact with the aromatic ring of salbutamol through hydrophobic interactions, which could contribute favorable van der Waals interaction energy by −2.41 kcal mol^{-1} in the WT system, as seen in Fig. 10 and Table S2. Inspection of Fig. 8 clearly shows that there are 11 residues in the mutant system that significantly favor binding, i.e., 3 more than in the WT. Most of the residues (viz., Trp109$^{3.28}$, Thr110$^{3.29}$,Val114$^{3.33}$, Phe193^{ECL2}, Phe289$^{6.51}$ and Asn312$^{7.39}$), observed to favor binding of salbutamol in the WT still retain favorable contribution to the binding, but with differences in the extent of their contributions (Fig. 8, Tables S2–S3). For example, the mutation weakens the contributions of Trp109$^{3.28}$ and Phe193^{ECL2} to binding, but increase contributions from Thr110$^{3.29}$, Val114$^{3.33}$ and Phe289$^{6.51}$ and Asn312$^{7.39}$ residues. In addition, residues Ser203$^{5.42}$, Ser204$^{5.43}$ and Ser207$^{5.46}$ in TM5 are not observed to provide any contribution to binding in the WT system within the scale of 110 ns simulation since their binding energies are calculated to be close to 0.0 kcal mol^{-1}. However, they contribute favorable binding energy by −2.13 kcal mol^{-1}, −0.75 kcal mol^{-1} and −3.27 kcal mol^{-1}, respectively, in the mutated system (see Fig. 8 and Table S2). The three serine residues have been considered to be important for agonist binding and activation of β2AR [62, 63].

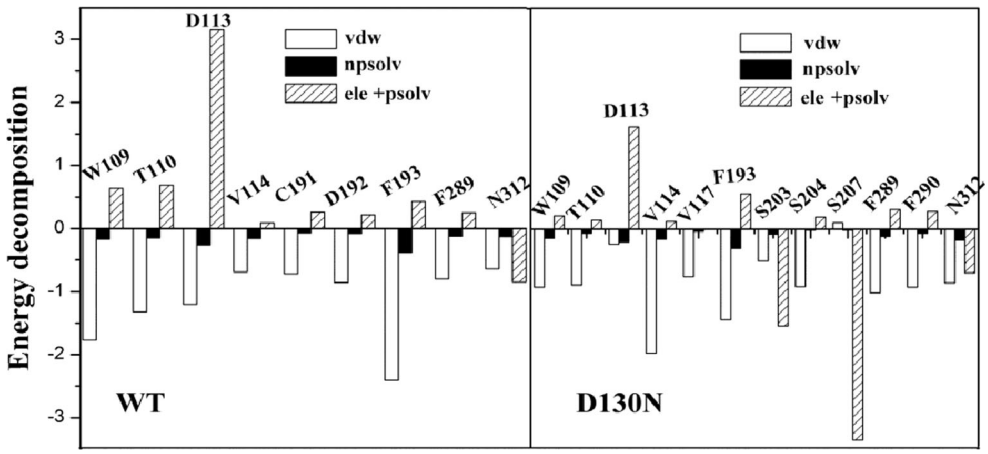

Fig. 9 Energy decomposition (in kcal mol^{-1}) into contribution from Van der Waals energy (*vdw*), the sum of non-bonded electrostatic energy and the polar contribution of solvation energy (*ele+psolv*) and the nonpolar term of solvation energy (*npsolv*) for residues whose absolute value of binding energy is larger than 0.5 kcal mol^{-1} for WT and mutant β2AR (D130N)

Some previous MD studies also reported the interaction of these three residues with some agonists and showed that the interaction of Ser207$^{5.46}$ with the agonist is strongest [23, 50]. In addition, mutation experiments showed that Ser207$^{5.46}$ has a larger impact on norepinephrine (a β2AR agonist) binding compared to Ser204$^{5.43}$ [64]. The observations derived from our study on the mutated β2AR further confirm that Ser207$^{5.46}$ plays a dominant role in binding the salbutamol agonist. Figure 9 and Table S3 further reveal that residues Ser203$^{5.42}$ and Ser207$^{5.46}$ in TM5 contribute to the binding energy mainly via electrostatic interaction by −3.13 kcal mol^{-1} and −4.06 kcal mol^{-1}, respectively. As revealed by Fig. 10, the mutation could favor TM5 to shift inward, enabling residues Ser203$^{5.42}$ and Ser207$^{5.46}$ to form a H-bond with the salbutamol agonist. It is the H-bonding induced by the mutation that contributes to the significant increase in the direct electrostatic interaction in the mutant form, thus enhancing binding strength. Observations from β2AR–Nb80 active crystal structures indicated that the greatest difference between the inactive and active structures in the ligand-binding site is an inward bulge of TM5 centered around Ser207$^{5.46}$ [12]. Also, some MD studies on β2AR-agonist complexes have reported that agonist binding would induce a conformational change of TM5 to allow the experimentally postulated interactions with residues Ser204$^{5.43}$ and Ser207$^{5.46}$ [23, 65].

Although residue Asp113$^{3.32}$ also forms a H-bond with the agonist in the mutant, which makes a large contribution (−12.73 kcal mol^{-1}) to the binding of salbutamol, the favorable contribution of the residue Asp113$^{3.32}$ resulting from the H-bond is completely offset by the unfavorable polar solvation energy (14.14 kcal mol^{-1}), as shown in Table S3. In addition, the favorable van der Waals contribution from Phe193 residue is weakened significantly by the mutation since the distance between the aromatic rings between Phe193^{ECL2} and the agonist is observed to become larger upon the conformation change of ECL2 caused by the mutation (see Fig. 10). However, the ECL2 conformational change brings the aromatic ring of Phe193^{ECL2} into close contact with the tertiary butyl group of the agonist (Fig. 10), which should contribute to a favorable hydrophobic interaction between the two groups and thus to binding.

In common with some previous MD studies on the interaction between β2AR and some agonists [23], we did not observe any significant contribution from Asn293$^{6.55}$ to binding in either WT or mutated β2AR, since its contributions to the binding energies were calculated to be −0.13 kcal mol^{-1} and −0.22 kcal mol^{-1} in the WT and mutated systems, respectively. Asn293$^{6.55}$ has been proposed to establish interactions with β-hydroxyl group agonists like norepinephrine [66]. But, some mutation studies have reported that non-catecholamine agonists do not interact strongly with Asn293$^{6.55}$ [67], in line with our results.

Conclusions

Using all-atom MD simulations and MM/GBSA free energy calculations, we studied the D130N mutation-induced activation of an inactive β2AR structure, and the role played by the D130N mutation in influencing drug binding. The results indicate that the mutation plays a negligible role in determining the compactness of the overall structure of β2AR, although it reduces stability to some extent. However, significant changes induced by the mutation were observed for some local but important regions, including regions near the mutation site, such as TM3, and regions far away from the mutation site, such as TM2 and TM7. In particular, the NPxxY region exhibited marked changes due to the mutation, which will contribute to the observed constitutive activation. The important ionic lock between Arg131$^{3.50}$ and Glu268$^{6.30}$ was observed to be dynamic in WT β2AR and seems not to play an essential role in stabilizing the inactive state of β2AR as it does in rhodopsin. However, the mutation completely disrupts the ionic lock, leading to the departure of TM3 from TM6. Thus, it is reasonable to assume that the active state of β2AR

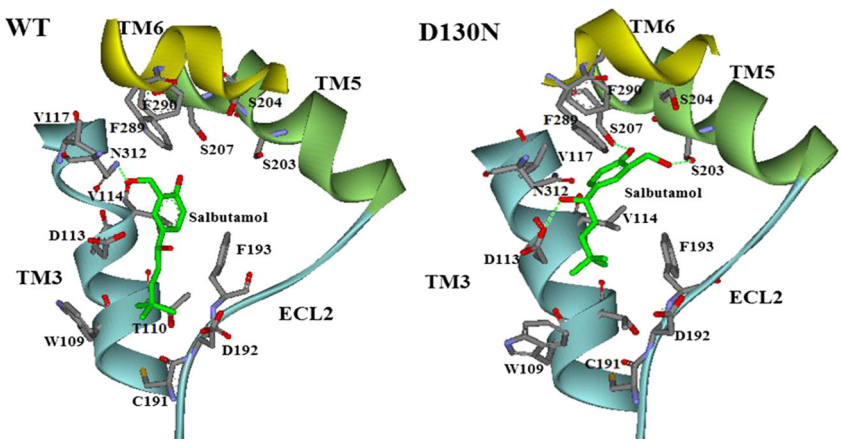

Fig. 10 Representative interactions between the agonist salbutamol and some high energy residues (|GBTOT|≥ 0.5 kcal mol^{-1}) of WT and mutant β2AR (D130N). *Sticks* denote salbutamol (in *green*) and some representatively high energy residues of β2AR. *Green dotted lines* H-bonding

can be characterized by the complete disruption of the ionic lock. The MD results also show that the mutation reduces the number of H-bonds and weakens the strength of some H-bonds. Accordingly, it gives rise to structural changes of regions involved in H-bonding, for example, the departure of TM7 from TM2. These observations show that the mutant already presents some structural features activated within the scale of the 110-ns simulation time, providing a structural basis for understanding the constitutive activity induced by the D130N mutation.

In addition, we used MM/GBSA calculations to study the interaction between the two β2AR types and the salbutamol agonist. The results indicated that residues making a significant contribution to binding come mainly from TM3, TM6, TM7 and ECL2 for the wild system within the scale of the 110-ns simulation time. However, the conformational changes induced by the mutation make TM5 significantly favor agonist binding, in contrast to WT β2AR. The main driving forces for binding in both systems are van der Waals and non-bonded electrostatic interactions. In particular, van der Waals interactions play a dominant role in drug binding for WT β2AR. However, the mutation significantly enhances the binding strength of β2AR with the salbutamol agonist, mainly through increasing electrostatic interactions rather than van der Waals interaction. The enhanced electrostatic interactions in the mutant type stem mainly from additional H-bonds formed between the agonist and residues Ser203$^{5.42}$ and Ser207$^{5.46}$ since the D130N mutation shifts TM5 inward to contact the agonist more closely. This observation suggests that modifications to polar (or H-bond) groups of drug ligands could play a significant role in influencing the efficacy of drugs used to treat diseases associated with the D130N mutation.

Acknowledgment This project was supported by the National Science Foundation of China (Grant No. 21273154, U1230121).

References

1. Takeda S, Kadowaki S, Haga T, Takaesu H, Mitaku S (2002) Identification of G protein-coupled receptor genes from the human genome sequence. FEBS Lett 520(1):97–101
2. Fredriksson R, Lagerström MC, Lundin L-G, Schiöth HB (2003) The G-protein-coupled receptors in the human genome form five main families. Phylogenetic analysis, paralogon groups, and fingerprints. Mol Pharmacol 63(6):1256–1272
3. Congreve M, Langmead CJ, Mason JS, Marshall FH (2011) Progress in structure based drug design for G protein-coupled receptors. J Med Chem 54(13):4283–4311
4. Gether U (2000) Uncovering molecular mechanisms involved in activation of G protein-coupled receptors. Endocr Rev 21(1):90–113
5. Arvanitakis L, Geras-Raaka E, Gershengorn MC (1998) Constitutively signaling G-protein-coupled receptors and human disease. Trends Endocrinol Metab 9(1):27–31
6. Thompson MD, Burnham WM, Cole DE (2005) The G protein-coupled receptors: pharmacogenetics and disease. Crit Rev Clin Lab Sci 42(4):311–392
7. Dryja TP, McGee TL, Reichel E, Hahn LB, Cowley GS, Yandell DW, Sandberg MA, Berson EL (1990) A point mutation of the rhodopsin gene in one form of retinitis pigmentosa. Nature 343(6256):364–366
8. Rao VR, Cohen GB, Oprian DD (1994) Rhodopsin mutation G90D and a molecular mechanism for congenital night blindness. Nature 367(6464):639–642
9. Robinson PR, Cohen GB, Zhukovsky EA, Oprian DD (1992) Constitutively active mutants of rhodopsin. Neuron 9(4):719–725
10. Themmen APN, Martens JWM, Brunner HG (1997) Gonadotropin receptor mutations. J Endocrinol 153(2):179–183
11. Van Sande J, Parma J, Tonacchera M, Swillens S, Dumont J, Vassart G (1995) Somatic and germline mutations of the TSH receptor gene in thyroid diseases. J Clin Endocrinol Metab 80(9):2577–2585
12. Rasmussen SG, Choi HJ, Fung JJ, Pardon E, Casarosa P, Chae PS, DeVree BT, Rosenbaum DM, Thian FS, Kobilka TS (2011) Structure of a nanobody-stabilized active state of the β2 adrenoceptor. Nature 469(7329):175–180
13. Cherezov V, Rosenbaum DM, Hanson MA, Rasmussen SG, Thian FS, Kobilka TS, Choi HJ, Kuhn P, Weis WI, Kobilka BK et al (2007) High-resolution crystal structure of an engineered human β2-adrenergic G protein-coupled receptor. Science 318(5854):1258–1265
14. Park JH, Scheerer P, Hofmann KP, Choe HW, Ernst OP (2008) Crystal structure of the ligand-free G-protein-coupled receptor opsin. Nature 454(7201):183–187
15. Warne T, Serrano-Vega MJ, Baker JG, Moukhametzianov R, Edwards PC, Henderson R, Leslie AGW, Tate CG, Schertler GFX (2008) Structure of a β1-adrenergic G-protein-coupled receptor. Nature 454(7203):486–491
16. Rasmussen SGF, Jensen AD, Liapakis G, Ghanouni P, Javitch JA, Gether U (1999) Mutation of a highly conserved aspartic acid in the β2 adrenergic receptor: constitutive activation, structural instability, and conformational rearrangement of transmembrane segment 6. Mol Pharmacol 56(1):175–184
17. Probst WC, Snyder LA, Schuster DI, Brosius J, Sealfon SC (1992) Sequence alignment of the G-protein coupled receptor superfamily. DNA Cell Biol 11(1):1–20
18. Xue WW, Pan DB, Yang Y, Liu HX, Yao XJ (2012) Molecular modeling study on the resistance mechanism of HCV NS3/4A serine protease mutants R155K, A156V and D168A to TMC435. Antivir Res 93(1):126–137
19. Yang M-J, Pang XQ, Zhang X, Han KL (2011) Molecular dynamics simulation reveals preorganization of the chloroplast FtsY towards complex formation induced by GTP binding. J Struct Biol 173(1):57–66
20. Zhu LJ, Yang W, Meng YY, Xiao XC, Guo YZ, Pu XM, Li ML (2012) Effects of organic solvent and crystal water on γ-chymotrypsin in acetonitrile media: observations from molecular dynamics simulation and DFT calculation. J Phys Chem B 116(10):3292–3304
21. Li MH, Luo Q, Li ZS (2010) Molecular dynamics study on the interactions of porphyrin with two antiparallel human telomeric quadruplexes. J Phys Chem B 114(18):6216–6224
22. Li Z, Cai YH, Cheng YK, Lu X, Shao YX, Li XS, Liu M, Liu PQ, Luo H-B (2013) Identification of novel phosphodiesterase-4D inhibitors prescreened by molecular dynamics-augmented modeling and validated by bioassay. J Chem Inf Model 53(4):972–981
23. Vilar S, Karpiak J, Berk B, Costanzi S (2011) In silico analysis of the binding of agonists and blockers to the β2-adrenergic receptor. J Mol Graph Model 29(6):809–817

24. Johnston JM, Filizola M (2011) Showcasing modern molecular dynamics simulations of membrane proteins through G protein-coupled receptors. Curr Opin Struc Biol 21(4):552–558
25. Rubenstein RC, Wong S, Ross E (1987) The hydrophobic tryptic core of the beta-adrenergic receptor retains Gs regulatory activity in response to agonists and thiols. J Biol Chem 262(34):16655–16662
26. Guex N, Peitsch MC (1997) SWISS-MODEL and the Swiss-PdbViewer: an environment for comparative protein modeling. Electrophoresis 18(15):2714–2723
27. Filizola M, Wang SX, Weinstein H (2006) Dynamic models of G-protein coupled receptor dimers: indications of asymmetry in the rhodopsin dimer from molecular dynamics simulations in a POPC bilayer. J Comput Aided Mol Des 20(7–8):405–416
28. Duan Y, Wu C, Chowdhury S, Lee MC, Xiong GM, Zhang W, Yang R, Cieplak P, Luo R, Lee T (2003) A point-charge force field for molecular mechanics simulations of proteins based on condensed-phase quantum mechanical calculations. J Comput Chem 24(16): 1999–2012
29. Jorgensen WL, Chandrasekhar J, Madura JD, Impey RW, Klein ML (1983) Comparison of simple potential functions for simulating liquid water. J Chem Phys 79(2):926–935
30. Wang JM, Wolf RM, Caldwell JW, Kollman PA, Case DA (2004) Development and testing of a general amber force field. J Comput Chem 25(9):1157–1174
31. Berendsen HJ, Postma JPM, van Gunsteren WF, DiNola A, Haak J (1984) Molecular dynamics with coupling to an external bath. J Chem Phys 81(8):3684–3690
32. Ryckaert J-P, Ciccotti G, Berendsen HJ (1977) Numerical integration of the cartesian equations of motion of a system with constraints: molecular dynamics of n-alkanes. J Comput Phys 23(3):327–341
33. York D, Darden T, Pedersen L, Anderson M (1993) Molecular dynamics simulation of HIV-1 protease in a crystalline environment and in solution. Biochemistry 32(6):1443–1453
34. Essmann U, Perera L, Berkowitz ML, Darden T, Lee H, Pedersen LG (1995) A smooth particle mesh Ewald method. J Chem Phys 103(19): 8577–8593
35. Humphrey W, Dalke A, Schulten K (1996) VMD: visual molecular dynamics. J Mol Graph 14(1):33–38
36. Morris GM, Huey R, Lindstrom W, Sanner MF, Belew RK, Goodsell DS, Olson AJ (2009) AutoDock4 and AutoDockTools4: automated docking with selective receptor flexibility. J Comput Chem 30(16): 2785–2791
37. Wang JM, Wang W, Kollman PA, Case DA (2006) Automatic atom type and bond type perception in molecular mechanical calculations. J Mol Graph Model 25(2):247–260
38. Miller BR III, McGee TD Jr, Swails JM, Homeyer N, Gohlke H, Roitberg AE (2012) MMPBSA.py: an efficient program for end-state free energy calculations. J Chem Theory Comput 8(9):3314–3321
39. Rastelli G, Degliesposti G, Del Rio A, Sgobba M (2009) Binding estimation after refinement, a new automated procedure for the refinement and rescoring of docked ligands in virtual screening. Chem Biol Drug Des 73(3):283–286
40. Lafont V, Armstrong AA, Ohtaka H, Kiso Y, Mario Amzel L, Freire E (2007) Compensating enthalpic and entropic changes hinder binding affinity optimization. Chem Biol Drug Des 69(6):413–422
41. Dror RO, Arlow DH, Maragakis P, Mildorf TJ, Pan AC, Xu HF, Borhani DW, Shaw DE (2011) Activation mechanism of the β2-adrenergic receptor. Proc Natl Acad Sci USA 108(46):18684–18689
42. Porter JE, Perez DM (1999) Characteristics for a salt-bridge switch mutation of the alpha(1b) adrenergic receptor—altered pharmacology and rescue of constitutive activity. J Biol Chem 274(49):34535–34538
43. Befort K, Zilliox C, Filliol D, Yue SY, Kieffer BL (1999) Constitutive activation of the δ opioid receptor by mutations in transmembrane domains III and VII. J Biol Chem 274(26):18574–18581
44. Huang P, Visiers I, Weinstein H, Liu-Chen L-Y (2002) The local environment at the cytoplasmic end of TM6 of the μ opioid receptor differs from those of rhodopsin and monoamine receptors: introduction of an ionic lock between the cytoplasmic ends of helices 3 and 6 by a L6. 30 (275) E mutation inactivates the μ opioid receptor and reduces the constitutive activity of its t6. 34 (279) k mutant. Biochemistry 41(40):11972–11980
45. Kim JM, Altenbach C, Kono M, Oprian DD, Hubbell WL, Khorana HG (2004) Structural origins of constitutive activation in rhodopsin: Role of the K296/E113 salt bridge. Proc Natl Acad Sci USA 101(34): 12508–12513
46. Dror RO, Arlow DH, Borhani DW, Jensen MØ, Piana S, Shaw DE (2009) Identification of two distinct inactive conformations of the β2-adrenergic receptor reconciles structural and biochemical observations. Proc Natl Acad Sci USA 106(12):4689–4694
47. Vanni S, Neri M, Tavernelli I, Rothlisberger U (2010) A conserved protonation-induced switch can trigger "ionic-lock" formation in adrenergic receptors. J Mol Biol 397(5):1339–1349
48. Gether U, Lin S, Ghanouni P, Ballesteros JA, Weinstein H, Kobilka BK (1997) Agonists induce conformational changes in transmembrane domains III and VI of the β2 adrenoceptor. EMBO J 16(22): 6737–6747
49. Wong CF, Kua J, Zhang Y, Straatsma TP, McCammon JA (2005) Molecular docking of balanol to dynamics snapshots of protein kinase A. Proteins 61(4):850–858
50. Bhattacharya S, Hall SE, Li H, Vaidehi N (2008) Ligand-stabilized conformational states of human β2 adrenergic receptor: insight into G-protein-coupled receptor activation. Biophys J 94(6):2027–2042
51. Ballesteros J, Kitanovic S, Guarnieri F, Davies P, Fromme BJ, Konvicka K, Chi L, Millar RP, Davidson JS, Weinstein H (1998) Functional microdomains in G-protein-coupled receptors the conserved arginine-cage motif in the gonadotropin-releasing hormone receptor. J Biol Chem 273(17):10445–10453
52. Barak LS, Tiberi M, Freedman NJ, Kwatra MM, Lefkowitz RJ, Caron MG (1994) A highly conserved tyrosine residue in G protein-coupled receptors is required for agonist-mediated beta 2-adrenergic receptor sequestration. J Biol Chem 269(4): 2790–2795
53. Barak LS, Menard L, Ferguson SS, Colapietro A-M, Caron MG (1995) The conserved seven-transmembrane sequence NP (X) 2, 3Y of the G-protein-coupled receptor superfamily regulates multiple properties of the. beta. 2-adrenergic receptor. Biochemistry 34(47): 15407–15414
54. Dixon R, Sigal I, Strader C (1988) Structure-function analysis of the β-adrenergic receptor. Cold Spring Harbor Symp Quant Biol 53: 487–497
55. Gabilondo AM, Krasel C, Lohse MJ (1996) Mutations of Tyr^{326} in the β_2-adrenoceptor disrupt multiple receptor functions. Eur J Pharmacol 307(2):243–250
56. Simpson LM, Wall ID, Blaney FE, Reynolds CA (2011) Modeling GPCR active state conformations: the β2-adrenergic receptor. Proteins 79(5):1441–1457
57. Warrell D, Robertson D, Howes JN, Conolly M, Paterson J, Beilin L, Dollery C (1970) Comparison of cardiorespiratory effects of isoprenaline and salbutamol in patients with bronchial asthma. BMJ 1(5688): 65–70
58. Ekue JK, Shanks R, Zaidi S (1971) Comparison of the effects of isoprenaline, orciprenaline, salbutamol and isoetharine on the cardiovascular system of anaesthetized dogs. Br J Pharmacol 43(1):23–31
59. Fraser CM, Chung FZ, Wang CD, Venter JC (1988) Site-directed mutagenesis of human beta-adrenergic receptors: substitution of aspartic acid-130 by asparagine produces a receptor with high-affinity agonist binding that is uncoupled from adenylate cyclase. Proc Natl Acad Sci USA 85(15):5478–5482
60. Deng NJ, Cieplak P (2009) Insights into affinity and specificity in the complexes of α-lytic protease and its inhibitor proteins: binding free

energy from molecular dynamics simulation. Phys Chem Chem Phys 11(25):4968–4981
61. Soriano-Ursúa MA, Trujillo-Ferrara JG, Correa-Basurto J, Vilar S (2013) Recent structural advances of β1 and β2 adrenoceptors yield keys for ligand recognition and drug design. J Med Chem 56(21): 8207–8223
62. Liapakis G, Ballesteros JA, Papachristou S, Chan WC, Chen X, Javitch JA (2000) The forgotten serine a critical role for Ser-203$^{5.42}$ in ligand binding to and Activation of the β_2-adrenergic receptor. J Biol Chem 275(48):37779–37788
63. Sato T, Kobayashi H, Nagao T, Kurose H (1999) Ser203 as well as Ser204 and Ser207 in fifth transmembrane domain of the human β2-adrenoceptor contributes to agonist binding and receptor activation. Brit J Pharmacol 128(2):272–274
64. Del Carmine R, Molinari P, Sbraccia M, Ambrosio C, Costa T (2004) "Induced-fit" mechanism for catecholamine binding to the β2-adrenergic receptor. Mol Pharmacol 66(2):356–363
65. Bhattacharya S, Vaidehi N (2010) Computational mapping of the conformational transitions in agonist selective pathways of a G-protein coupled receptor. J Am Chem Soc 132(14):5205–5214
66. Wieland K, Zuurmond HM, Krasel C, Ijzerman AP, Lohse MJ (1996) Involvement of Asn-293 in stereospecific agonist recognition and in activation of the beta 2-adrenergic receptor. Proc Natl Acad Sci USA 93(17):9276–9281
67. Hannawacker A, Krasel C, Lohse MJ (2002) Mutation of Asn293 to Asp in transmembrane helix VI abolishes agonist-induced but not constitutive activity of the β2-adrenergic receptor. Mol Pharmacol 62(6):1431–1437